

# Exact and Semiclassical Density Matrix of a Particle Moving in a Barrier Potential with Bound States

Franz Josef Weiper, Joachim Ankerhold, and Hermann Grabert

*Fakultät für Physik, Albert-Ludwigs-Universität Freiburg, Hermann-Herder-Straße 3,*

*D-79104 Freiburg im Breisgau, Germany*

(October 11, 1995)

## Abstract

We present a barrier potential with bound states that is exactly solvable and determine the eigenfunctions and eigenvalues of the Hamiltonian. The equilibrium density matrix of a particle moving at temperature  $T$  in this nonlinear barrier potential field is determined. The exact density matrix is compared with the result of the path integral approach in the semiclassical approximation. For opaque barriers the simple semiclassical approximation is found to be sufficient at high temperatures while at low temperatures the fluctuation paths may have a caustic depending on temperature and endpoints. Near the caustics the divergence of the simple semiclassical approximation of the density matrix is removed by a nonlinear fluctuation potential. For opaque barriers the improved semiclassical approximation is again in agreement with the exact result. In particular, bound states and the form of resonance states are described accurately by the semiclassical approach.

PACS numbers: 82.20.Kh, 03.65.Sq, 05.30.-d

## I. INTRODUCTION

The semiclassical approximation to quantum mechanical problems is useful in a large variety of contexts. In chemistry and physics this approach becomes more prevalent for many reasons. For instance, semiclassical methods are efficient for the calculation of highly excited states, for which direct quantum mechanical calculations become difficult. The semiclassical approach also offers conceptual insights into the dynamics of many systems that are not easily extracted directly from the quantum mechanical treatment [1]. Finally, physical quantities of systems with barrier potentials can be calculated in the semiclassical limit, that corresponds to a large barrier height or a large barrier width [2]. Here we study a system with a nonlinear potential field that has a barrier and an adjacent well. For the specific potential field considered, the classical equation of motion as well as the corresponding Schrödinger equation can be solved exactly. Therefore, the model can be used to test the quality of approximations to which one has to resort for most realistic potential fields.

The imaginary time path integral approach provides a consistent scheme for the semiclassical approximation of several quantities in statistical mechanics [3]. It has been noted already 25 years ago [4] that classical paths methods offer facile techniques to determine the semiclassical approximation of the equilibrium density matrix or the partition function. In the last few years the formulation of quantum statistical mechanics based on the centroid density, originally suggested by Feynman, was studied extensively [5]. Although this formulation allows for highly accurate approximations for the partition function, the centroid density has the same physical interpretation as the density matrix only in the high temperature limit. The simple semiclassical approximation for the density matrix studied in the past [4] becomes exact at high temperature, however for coordinates near critical values divergencies arise when the temperature is lowered [6]. Well-known as the problem of caustics, these divergencies reflect the fact that new classical paths become available. In the region, where these paths emerge, one has to improve upon the simple semiclassical approximation

and evaluate non-Gaussian fluctuation integrals [6].

In this article we compare the exact equilibrium density matrix with the improved semiclassical approximation. First, in section 2 we calculate the exact equilibrium density matrix using analytic solutions of the Schrödinger equation. The simple semiclassical approximation is evaluated in section 3. In section 4 we present an improved semiclassical approximation for the density matrix which remains valid near the caustics. Section 5 presents semiclassical results for bound and resonance states.

## II. EXACT EQUILIBRIUM DENSITY MATRIX

We consider the thermal equilibrium state of a quantum system with the asymmetric barrier potential

$$V_0(X) = U_0 \frac{A + B \sinh(X/L_0)}{\cosh^2(X/L_0)}, \quad (1)$$

where  $A$  and  $B$  are dimensionless coefficients,  $L_0$  denotes the typical range of the potential and  $U_0$  the energy scale. The Schrödinger equation with potential (1) will be seen to be exactly solvable. In particular, for  $B = 0$  we recover the symmetric Eckart potential [7,8].

The antisymmetric part of the potential proportional to  $\sinh(X/L_0)/\cosh^2(X/L_0)$  is different from the  $\tanh(X/L_0)$  term familiar from the work by Rosen and Morse [9]. This leads to important qualitative differences in the shapes of these exactly solvable potentials. As seen from Fig. 1, the potential (1) always approaches the same limiting value for  $X \rightarrow \pm\infty$ , and for  $B \neq 0$  it displays a barrier with an adjacent well. The fact that the potential is a genuine scattering potential decaying exponentially for large  $|X|$  and the barrier-well form distinguish (1) from other exactly solvable smooth potentials.

### A. The Schrödinger Equation

The Schrödinger equation of a quantum mechanical particle moving in the potential (1) may be written as

$$\left[ -\frac{1}{2} \frac{d^2}{dx^2} + V(x) \right] \Psi(x) = \epsilon \Psi(x), \quad (2)$$

with the scaled potential

$$V(x) = \frac{a + b \sinh(x)}{2 \cosh^2(x)}. \quad (3)$$

In (2) and (3), we have introduced the dimensionless quantities

$$\begin{aligned} x &= X/L_0 & \epsilon &= mL_0^2 E/\hbar^2, \\ a &= 2mU_o L_0^2 A/\hbar^2, & b &= 2mU_o L_0^2 B/\hbar^2. \end{aligned} \quad (4)$$

For later purpose we also introduce the dimensionless inverse temperature

$$\beta = \hbar^2/mL_0^2 k_B T, \quad (5)$$

where  $k_B$  is the Boltzmann constant [10].

With the transformation  $y = \sinh(x)$  [11] the Schrödinger equation (2) takes the form

$$\Psi''(y) + \frac{y}{1+y^2} \Psi'(y) + \left[ \frac{2\epsilon}{1+y^2} - \frac{a+by}{(1+y^2)^2} \right] \Psi(y) = 0. \quad (6)$$

This second order differential equation has three singular points at  $i$ ,  $-i$ , and  $\infty$ . It can be reduced to its canonical form with the ansatz

$$\Psi(y) = (y+i)^{\frac{1}{4}+\frac{1}{4}s} (y-i)^{\frac{1}{4}+\frac{1}{4}s^*} F(y), \quad (7)$$

where

$$s = \sqrt{1-4a+i4b} = s' + is'', \quad (8)$$

with the real and imaginary parts given by

$$\begin{aligned} s' &= \left\{ \frac{1}{2} \left[ (1-4a)^2 + (4b)^2 \right]^{\frac{1}{2}} + \frac{1-4a}{2} \right\}^{\frac{1}{2}} \\ s'' &= \text{sign}(b) \left\{ \frac{1}{2} \left[ (1-4a)^2 + (4b)^2 \right]^{\frac{1}{2}} - \frac{1-4a}{2} \right\}^{\frac{1}{2}}. \end{aligned} \quad (9)$$

Inserting (7) into (6), we obtain with the substitution

$$z = \frac{1}{2} - i\frac{y}{2} \quad (10)$$

a hypergeometric differential equation for  $F(z)$

$$z(1-z)F''(z) + [\gamma - (\alpha + \alpha^* + 1)z]F'(z) - \alpha\alpha^*F(z) = 0. \quad (11)$$

Here, the coefficients  $\alpha$  and  $\gamma$  are given by

$$\begin{aligned} \alpha &= \frac{1}{2} + \frac{s'}{2} + i\sqrt{2\epsilon} \\ \gamma &= 1 + \frac{1}{2}s. \end{aligned} \quad (12)$$

A solution of (11) is given by the hypergeometric function  ${}_2F_1(\alpha, \alpha^*; \gamma; z)$  [12]. The corresponding solution of equation (6) reads

$$\Psi(z) = [i2z]^{\frac{1}{4} + \frac{1}{4}s} [i2(z-1)]^{\frac{1}{4} + \frac{1}{4}s^*} {}_2F_1(\alpha, \alpha^*; \gamma; z). \quad (13)$$

This solution is defined in the complex plane for  $|z| \leq 1$ , i.e. for coordinates  $|x| \leq \text{arcosh}(2)$ . Beyond this region the solution is analytically continued by means of the formula [12]

$$\begin{aligned} {}_2F_1(\alpha, \alpha^*; \gamma; z) &= \frac{\Gamma(\gamma)\Gamma(\alpha^* - \alpha)}{\Gamma(\alpha^*)\Gamma(\gamma - \alpha)} (-z)^{-\alpha} {}_2F_1(\alpha, 1 - \gamma + \alpha; 1 - \alpha^* + \alpha; \frac{1}{z}) \\ &+ \frac{\Gamma(\gamma)\Gamma(\alpha - \alpha^*)}{\Gamma(\alpha)\Gamma(\gamma - \alpha^*)} (-z)^{-\alpha^*} {}_2F_1(\alpha^*, 1 - \gamma + \alpha^*; 1 - \alpha + \alpha^*; \frac{1}{z}). \end{aligned} \quad (14)$$

This way we have found an exact solution of the Schrödinger equation defined in the whole domain of  $x$ . Of course, physically acceptable solutions have to satisfy proper boundary conditions.

Let us first consider the case  $\epsilon > 0$ , i.e. a typical scattering situation. Since the potential (3) decays exponentially for large  $|x|$ , the wave function  $\Psi(x)$  should reduce to plane wave states at large coordinates. For  $x \rightarrow \pm\infty$  the argument  $1/z$  in (14) vanishes and one can show that the asymptotic behavior of the solution (13) is indeed of the form

$$\Psi(x \rightarrow \pm\infty) = A_{\pm} \exp[-i\sqrt{2\epsilon}(\pm x)] + B_{\pm} \exp[i\sqrt{2\epsilon}(\pm x)], \quad (15)$$

with energy dependent amplitudes

$$A_{\pm} = \frac{\Gamma(\gamma)\Gamma(\alpha^* - \alpha)}{\Gamma(\alpha^*)\Gamma(\gamma - \alpha)} \exp \left\{ \frac{1 + s'}{2} \left[ \ln(2) \mp i\frac{\pi}{2} \right] \pm \left[ \frac{\pi}{2} \pm 2i \ln(2) \right] \sqrt{2\epsilon} - \left( \frac{\pi}{2} \mp \frac{\pi}{2} \right) s'' \right\} \quad (16)$$

and

$$B_{\pm} = \frac{\Gamma(\gamma)\Gamma(\alpha - \alpha^*)}{\Gamma(\alpha)\Gamma(\gamma - \alpha^*)} \exp \left\{ \frac{1 + s'}{2} \left[ \ln(2) \mp i\frac{\pi}{2} \right] \mp \left[ \frac{\pi}{2} \pm 2i \ln(2) \right] \sqrt{2\epsilon} - \left( \frac{\pi}{2} \mp \frac{\pi}{2} \right) s'' \right\}. \quad (17)$$

Accordingly, the complex conjugate solution  $\Psi^*(x)$  behaves asymptotically as

$$\Psi^*(x \rightarrow \pm\infty) = A_{\pm}^* \exp(\pm i\sqrt{2\epsilon}x) + B_{\pm}^* \exp(\mp i\sqrt{2\epsilon}x), \quad (18)$$

We superimpose these two solutions to wave functions

$$\Phi_{\pm}(x) = u_{\pm}\Psi(x) + v_{\pm}\Psi^*(x) \quad (19)$$

with the asymptotic behavior

$$\Phi_{\pm}(x \rightarrow \pm\infty) = \exp(\pm i\sqrt{2\epsilon}x), \quad (20)$$

describing outgoing scattering waves. The coefficients  $u_{\pm}$  and  $v_{\pm}$  are found to read

$$\begin{aligned} u_{\pm} &= \frac{B_{\pm}^*}{|B_{\pm}|^2 - |A_{\pm}|^2} \\ v_{\pm} &= -\frac{A_{\pm}}{|B_{\pm}|^2 - |A_{\pm}|^2}. \end{aligned} \quad (21)$$

The asymptotic behavior of  $\Phi_{\pm}(x)$  for  $x \rightarrow \mp\infty$  is then given by

$$\Phi_{\pm}(x \rightarrow \mp\infty) = \frac{1}{t_{\pm}(\epsilon)} \exp(\pm i\sqrt{2\epsilon}x) + \frac{r_{\pm}(2\epsilon)}{t_{\pm}(\epsilon)} \exp(\mp i\sqrt{2\epsilon}x), \quad (22)$$

where the transmission and reflection amplitudes  $t_{\pm}(\epsilon)$  and  $r_{\pm}(\epsilon)$  are given by

$$\begin{aligned} t_{\pm}(\epsilon) &= \frac{|B_{\pm}|^2 - |A_{\pm}|^2}{B_{\pm}^*A_{\mp} - B_{\mp}^*A_{\pm}} \\ r_{\pm}(\epsilon) &= \frac{B_{\pm}^*B_{\mp} - A_{\mp}^*A_{\pm}}{B_{\pm}^*A_{\mp} - B_{\mp}^*A_{\pm}}. \end{aligned} \quad (23)$$

The amplitudes  $t_+$  and  $r_+$  can be expressed in terms of  $r_-$  and  $t_-$  by

$$\begin{aligned} t_+ &= t_- \\ r_+ &= -r_-^*t_-/t_-^*. \end{aligned} \quad (24)$$

Clearly,  $t_{\pm}(\epsilon)\Phi_{\pm}(x)$  describe the stationary scattering of particles incident from the far left and right, respectively, with energy  $\epsilon$  and unit amplitude. Inserting the explicit result for the amplitude factors  $A_{\pm}$  and  $B_{\pm}$ , the transmission probability  $T(\epsilon) = |t_{\pm}(\epsilon)|^2$  is found to read

$$T(\epsilon) = \exp(\pi s'') \frac{\sinh^2 \left( \pi \sqrt{2\epsilon} + \frac{1}{2} \ln \left\{ \frac{\cosh \left[ \pi \left( \frac{\sqrt{2\epsilon} - s''}{2} \right) \right]}{\cosh \left[ \pi \left( \frac{\sqrt{2\epsilon} + s''}{2} \right) \right]} \right\} \right)}{\sinh^2 \left( \pi \sqrt{2\epsilon} \right) + \cos^2 \left( \frac{\pi}{2} s' \right)}. \quad (25)$$

For the symmetric case,  $b = 0$ , this result agrees with the known transmission probability for the Eckart potential [7,8].

Fig. 2 shows  $T$  as a function of  $b$  for fixed  $a$  and various energies. Note that for small energies the transmission probability can be raised by increasing the asymmetry parameter  $b$ . While with increasing  $b$  the barrier height increases too, the width of the barrier decreases leading to a maximum of the transition probability at finite  $b$ .

For  $\epsilon < 0$  the solutions of the Schrödinger equation are not bound, except for the case when  $\epsilon$  coincides with an energy eigenvalue. To calculate the energy eigenvalues of the potential we seek for poles of the  $S$ -matrix at negative energies, or poles of the transmission amplitude, respectively. This way we get for the bound state spectrum

$$\epsilon_n = -\frac{1}{8} [-(2n + 1) + s']^2, \quad (26)$$

in which  $n = 0, 1, \dots, n_{\max}$  where  $n_{\max}$  is the largest integer with  $2n + 1 < s'$ . From (2) and (11) the corresponding bound states are obtained as

$$\psi_n(z) = \frac{1}{\sqrt{N_n}} [i2z]^{\frac{1}{4} - \frac{1}{4}s} [i2(z-1)]^{\frac{1}{4} - \frac{1}{4}s^*} {}_2F_1 \left( 1 + n - s', -n; 1 - \frac{s}{2}; z \right), \quad (27)$$

where  $z$  is given by (10) and  $N_n$  is a normalization constant. Note that the second coefficient of the hypergeometric function is a negative integer. Therefore the hypergeometric function is a polynomial of  $z$  of order  $n$ . Of course,  $\psi_n$  is a complex function but one can show that the real and the imaginary parts of  $\psi_n$  differ only by a constant. Hence, the eigenvalue  $\epsilon_n$  is not degenerate. Clearly bound states only exist for  $s' \geq 1$ .

In the symmetric case  $b = 0$  bound states only occur for  $a < 0$  and the spectrum has the well known form [8]

$$\epsilon_n = -\frac{1}{8} \left\{ -(2n + 1) + \{1 + 4a\}^{\frac{1}{2}} \right\}^2. \quad (28)$$

For  $a = 0$  the potential (1) becomes antisymmetric and the energy eigenvalues of the bound states are

$$\epsilon_n = -\frac{1}{8} \left( -(2n + 1) + \left\{ \frac{1}{2} + \frac{1}{2} [1 + (4b)^2]^{\frac{1}{2}} \right\}^{\frac{1}{2}} \right)^2. \quad (29)$$

In both of these cases there exists at least one bound state for arbitrary  $a$  and  $b$ , respectively. If  $a > 0$  and  $b \neq 0$  the condition for having at least one bound state is  $b \geq \sqrt{a}$ .

Fig. 3 shows the transmission probability  $T$  as a function of  $a \leq 0$  for fixed energy and various values of the asymmetry parameter  $b$ . The transmission probability for  $b = 0$  has maxima exactly at those points where new bound states are formed, i.e. where  $\epsilon_{n_{max}}$  is equal to zero. Then, for all energies the transmission probability reaches 1 and an incoming wave function is completely transmitted. We note that a similar behavior of the transmission probability is also found for  $b \neq 0$  and  $a \geq 0$ , however, in general the position and the height of the maxima depend on the values of  $\epsilon$  and  $b$ . For instance, for  $\epsilon \rightarrow 0$  the transmission probability has a maximum for  $a = 1$  at  $b = 1$  (Fig.2) where  $n_{max} = 0$ . Further maxima occur for  $s' = 2n + 1$ , i.e. for  $a = 1$ , at those values of  $b$  where

$$b = \frac{2n + 1}{2} \sqrt{(2n + 1)^2 + 3}. \quad (30)$$

The transmission probability for  $s' = 2n + 1$  reads in the limit  $\epsilon \rightarrow 0$

$$T(0)|_{s'=2n+1} = 1 / \cosh^2(\pi s''/2). \quad (31)$$

## B. The Equilibrium Density Matrix

We assume now that the energy of particles incident from the far left and right is thermally distributed. If we use the dimensionless formulation introduced in (4) and (5), the



state of the system is then described by the equilibrium density matrix at inverse temperature  $\beta$  which has the coordinate representation

$$\rho_\beta(x, x') = \frac{1}{Z} \langle x | \exp(-\beta \hat{H}) | x' \rangle \quad (32)$$

where  $Z$  is an appropriate normalization constant and  $\hat{H}$  the Hamilton operator from (2). Using a complete set  $\{\Phi_\epsilon\}$  of orthonormal eigenfunctions of the Hamiltonian with

$$\int_0^\infty d\epsilon \Phi_\epsilon^*(x) \Phi_\epsilon(x') + \sum_{n=0}^{N_{max}} \Phi_n^*(x) \Phi_n(x') = \delta(x - x') \quad (33)$$

one gets

$$\rho_\beta(x, x') = \frac{1}{Z} \left[ \int_0^\infty d\epsilon \exp(-\beta\epsilon) \Phi_\epsilon^*(x) \Phi_\epsilon(x') + \sum_{n=0}^{n_{max}} \exp(-\beta\epsilon_n) \Phi_n^*(x) \Phi_n(x') \right]. \quad (34)$$

Hence, the density matrix at given inverse temperature  $\beta$  as a function of  $x$  and  $x'$  is reduced to a sum over the discrete spectrum and an integration about the continuous spectrum which both has to be done numerically.

The bound states in (34) are given by (27). The scattering states  $\Phi_\epsilon$  are constructed appropriately from the solutions  $\Psi(x)$  in (13). According to (19) we have for given energy two independent scattering states of the system with the asymptotic behavior given by (20) and (22). Hence,  $t\Phi_+/\sqrt{2\pi}$  and  $t\Phi_-/\sqrt{2\pi}$  form an orthonormal set of wave functions for  $\epsilon > 0$ . Thus, according to (34), the diagonal part of the density matrix, i.e. the position distribution  $P(x) = \rho_\beta(x, x)$ , reads

$$P(x) = \frac{1}{Z} \left[ \int_0^\infty \frac{dk}{2\pi} \exp(-\beta k^2/2) T(k) \left( |\Phi_+(k, x)|^2 + |\Phi_-(k, x)|^2 \right) + \sum_{n=0}^{n_{max}} \exp(-\beta\epsilon_n) \frac{|\psi_n(x)|^2}{N_n} \right], \quad (35)$$

where we have introduced the dimensionless momentum  $k$  by

$$\epsilon = \frac{1}{2} k^2. \quad (36)$$

Performing the integration (35) for various values of  $a$  and  $b$  one sees that for large values of  $a$  and  $b$ , corresponding to potential fields with a large height or depth, the numerics becomes rather nontrivial because of the strongly oscillating hypergeometric functions. The potential (3) has extrema

$$V^\pm = \frac{1}{4} \left( a \pm \sqrt{a^2 + b^2} \right) \quad (37)$$

at

$$x^\pm = \operatorname{arsinh} \left[ -\frac{a}{b} \pm \sqrt{\left(\frac{a}{b}\right)^2 + 1} \right]. \quad (38)$$

For increasing  $a$  and  $b$  the absolute values of  $V^\pm$  become large. In dimensional units this corresponds to the fact that the extrema of the potential become large compared to the quantum mechanical energy scales of the system. The latter are given by the ground state energies of harmonic oscillators with frequencies proportional to the curvature of the potential in the well and at the barrier top, respectively. Now, for large  $V^\pm$  we have the typical situation where a semiclassical approximation should be valid. Thereby, the semiclassical expansion in powers of  $\hbar$  in dimensional units corresponds to an expansion in powers of  $1/\sqrt{2V^\pm}$  in the dimensionless formulation introduced above. We will show in the following that the usual WKB–approximation is indeed sufficient except for a small parameter range where the simple semiclassical approximation has to be improved upon. In particular, this improved semiclassical result can be handled numerically very simply and provides an excellent approximation for the exact density matrix in the region where the numerical evaluation of Eq. (35) becomes difficult.

### III. SEMICLASSICAL DENSITY MATRIX

#### A. Path Integral and Semiclassical Approximation

The dimensionless coordinate representation of the equilibrium density matrix of a quantum particle moving in the potential  $V(x)$  may be written as an imaginary time path integral [3]

$$\rho_\beta(x, x') = \int \mathcal{D}[x] e^{-S[x]}. \quad (39)$$

Here, the functional integral is over all paths  $x(\tau)$ ,  $0 \leq \tau \leq \beta$  with  $x(0) = x$  and  $x(\beta) = x'$ . Each path is weighted by its Euclidean action

$$S[x] = \int_0^\beta d\tau \left[ \frac{1}{2} \dot{x}^2 + V(x) \right]. \quad (40)$$

To evaluate the path integral in a semiclassical expansion we first determine the maximum of the weighting factor, that is the minimum of  $S[x]$ . This is given by the classical action  $S[x_{cl}]$ , where  $x_{cl}$  is the classical path solving the classical equation of motion following from Hamilton's principle  $\delta S[x] = 0$ . An arbitrary path in (39) reads

$$x(\tau) = x_{cl}(\tau) + y(\tau), \quad (41)$$

where  $y(\tau)$  describes the quantum fluctuations about the classical path. The fluctuations have to fulfill periodic boundary conditions  $y(0) = y(\beta) = 0$ . Using (41) the full action is then expanded around its minimum. This way the dominant part is separated off and one is left with a functional integral over periodic paths. In the simple semiclassical or WKB–approximation, the expansion of the full action is truncated after the second order term leading to an exactly solvable Gaussian path integral [3].

If there exists a set  $\{x_{cl}^\alpha\}$  of classical trajectories in  $V(x)$ , this procedure must be performed for each  $x_{cl}^\alpha$ , and all contributions are summed to yield the semiclassical density matrix

$$\rho_\beta(x, x') = \sum_\alpha \frac{1}{\sqrt{J_\alpha}} e^{-S[x_{cl}^\alpha]}, \quad (42)$$

where  $J_\alpha = \det\{\delta^2 S[x]/\delta x(\tau_1)\delta x(\tau_2)|_{x=x_{cl}^\alpha}\}$  is the determinant describing the Gaussian integral over the quantum fluctuations [3].  $J_\alpha$  is given by the product of eigenvalues  $\{\Lambda_n\}$  of the second order variational operator  $\delta^2 S[x]/\delta x(\tau_1)\delta x(\tau_2)|_{x=x_{cl}^\alpha}$  as

$$J_\alpha = 2\pi\beta \prod_n (N \Lambda_n^\alpha) \quad (43)$$

where  $N$  is an appropriate normalization constant. As long as the second order variational operator is positive definite, i.e.  $\Lambda_n > 0$  for all  $n$ , the Gaussian approximation gives the leading order fluctuation term. But a problem arises if one of the eigenvalues  $\Lambda_n$  tends to zero, e.g. as the temperature is lowered. Then, the quantum fluctuations of this mode

become arbitrarily large and the simple semiclassical approximation breaks down. Generally, the vanishing of an eigenvalue  $\Lambda_n$  defines a point where new minimal action paths in the potential  $V(x)$  become possible. This is well-known as the problem of caustics. For our purposes we also use another representation of  $J_\alpha$  equivalent to (43). One finds [3]

$$J_\alpha = 2\pi \dot{x}_{cl}^\alpha(\beta) \dot{x}_{cl}^\alpha(0) \int_0^\beta \frac{1}{[\dot{x}_{cl}^\alpha(\tau)]^2} d\tau \quad (44)$$

where  $\dot{x}$  denotes the time derivative  $dx/d\tau$ . This way the semiclassical approximation is completely determined by the classical paths.

## B. Classical Paths

In the following we first investigate the classical motion in the inverted potential  $-V(x)$ . Afterwards, the corresponding classical action and the contribution of the quantum fluctuations about the classical path are determined.

The Euclidean energy of the system reads

$$\epsilon = -\frac{1}{2} \dot{x}^2 + \frac{a + b \sinh(x)}{2 \cosh^2(x)}. \quad (45)$$

The solution of the classical equation of motion for fixed  $\epsilon$  is given by

$$x(\tau) = \operatorname{arsinh} \left\{ \frac{b}{4\epsilon} + \sqrt{\frac{b^2}{16\epsilon^2} + \frac{a}{2\epsilon} - 1} \sin \left[ \sqrt{2\epsilon} (\tau + \beta_0) \right] \right\}, \quad (46)$$

where  $\beta_0$  is an integration constant. The parameters  $\epsilon$  and  $\beta_0$  of the solution are determined by the boundary conditions  $x(0) = x$ ,  $x(\beta) = x'$  leading to

$$\begin{aligned} \sinh(x) &= \frac{b}{4\epsilon} + \sqrt{\frac{b^2}{16\epsilon^2} + \frac{a}{2\epsilon} - 1} \sin[\sqrt{2\epsilon}\beta_0] \\ \sinh(x') &= \frac{b}{4\epsilon} + \sqrt{\frac{b^2}{16\epsilon^2} + \frac{a}{2\epsilon} - 1} \sin[\sqrt{2\epsilon}(\beta + \beta_0)]. \end{aligned} \quad (47)$$

Due to the sine function in (47) one expects that there may be more than one trajectory connecting the endpoints for a given inverse temperature or “time”  $\beta$ . The maximum amplitude  $x_m$  of these path is then determined by  $V(x_m) = \epsilon$ . Note that  $\epsilon$  may be negative. Therefore  $\beta_0$  is in general an imaginary phase and due to the relation  $\sin(ix) = i \sinh(x)$  the oscillatory solution may change into a part of an unbounded motion.

### 1. Symmetric Barrier Potential ( $b = 0$ )

Let us first consider the motion of a classical particle in the inverted symmetric barrier potential ( $a > 0, b = 0$ ) [13]. The boundary conditions (47) then reduce to

$$\begin{aligned}\sinh(x) &= \sqrt{\frac{a-2\epsilon}{2\epsilon}} \sin[\sqrt{2\epsilon}\beta_0] \\ \sinh(x') &= \sqrt{\frac{a-2\epsilon}{2\epsilon}} \sin[\sqrt{2\epsilon}(\beta + \beta_0)].\end{aligned}\quad (48)$$

The simplest case is obtained for the boundary condition  $x = x' = x^+ = 0$  where  $x^+$  is the coordinate (38) at the barrier top. Then, for short times, i.e. high temperatures, there exists only the constant solution  $x(\tau) = 0$  of (46) with  $\epsilon = V^+ = a/2$ . When the temperature is lowered two new solutions with  $\epsilon = \pi^2/2\beta^2$  and  $\beta_0 = 0, \beta$  arise for  $\beta \geq \beta_c = \pi/\sqrt{2V^+}$ . These solutions describe oscillations in the well of the inverted potential. It will be shown below that the constant path, which is stable for high temperatures, becomes unstable for times  $\beta > \beta_c$  where the newly emerging trajectories with  $x_m \neq 0$  are stable (cf. Fig. 4). This change of stability is typical for a Hopf bifurcation.

For  $x = x' \neq 0$  the bifurcation scenario is perturbed (see Fig. 4). For  $\beta < \beta_c$  one has only one stable path that continuously extends also to the region  $\beta > \beta_c$ . For some critical value  $\tilde{\beta}_c$  two new branches emerge describing an oscillation to the other side of the well in the inverted potential. The solution of smaller amplitude is unstable while the other one is stable. The critical value  $\tilde{\beta}_c$  increases with increasing  $|x| = |x'|$ . For endpoints within the harmonic range of the potential, where  $|x| \ll 1$ , the critical temperature  $\tilde{\beta}_c$  remains close to  $\beta_c$ .

Further bifurcations appear in an analog way near  $\beta = n\beta_c$ ,  $n = 1, 2, 3, \dots$ . For  $x = x' = 0$  we obtain from (48) the parameters of the two trajectories bifurcating at  $\beta = n\beta_c$

$$\begin{aligned}b &= 0, \beta/n \\ \sqrt{2\epsilon}\beta &= n\pi \quad n = 1, 2, 3, \dots\end{aligned}\quad (49)$$

The parameters of the corresponding trajectories for  $x = x' \neq 0$  describing the perturbed bifurcation near  $\beta = n\beta_c$  are determined by

$$\begin{aligned}\sin[\sqrt{2\epsilon}(\beta + \beta_0)] &= \sin[\sqrt{2\epsilon}\beta_0] \\ \sqrt{2\epsilon}(\beta + \beta_0) &= \sqrt{2\epsilon}\beta_0(-1)^n + n\pi.\end{aligned}\tag{50}$$

For  $n$  odd the newly emerging paths are periodic in coordinate space with  $x(\beta) = x(0)$  and  $\dot{x}(\beta) = -\dot{x}(0)$ , while for  $n$  even they are even periodic in phase space with  $x(\beta) = x(0)$ ,  $\dot{x}(\beta) = \dot{x}(0)$ .

In the general case  $x \neq x' \neq 0$  there is again a similar bifurcation sequence as the temperature is lowered. However, for high temperatures, i.e. for very small times  $\beta$ , the solution of (48) connecting  $x$  and  $x'$  is a segment of an unbounded trajectory in the inverted potential with  $\epsilon < 0$ .

## 2. Asymmetric Barrier Potential ( $a, b > 0$ )

Now, we investigate the general case  $a \neq b \neq 0$  where we assume  $a, b > 0$ . The classical motion in the other cases  $a, b < 0$  and  $a < 0, b > 0$  as well as  $a > 0, b < 0$  is readily obtained in an analog way.

Let us consider the boundary condition  $x = x'$  in some detail. Then (47) can be transformed to read

$$\begin{aligned}\sqrt{2\epsilon}(\beta + \beta_0) &= \sqrt{2\epsilon}\beta_0(-1)^n + n\pi, \\ x(0) &= x.\end{aligned}\tag{51}$$

For  $n$  odd the phase  $\beta_0$  can easily be determined from (51) and the energy  $\epsilon$  follows from

$$\sinh(x) = \frac{b}{4\epsilon} + (-1)^n \sqrt{\frac{b^2}{16\epsilon^2} + \frac{a}{2\epsilon} - 1} \cos\left(\sqrt{2\epsilon}\frac{\beta}{2}\right)\tag{52}$$

For  $n$  even the energy  $\epsilon$  is given by  $\sqrt{2\epsilon}\beta = n\pi$  and the phase  $\beta_0$  is determined by

$$\sinh(x) = \frac{b\beta^2}{2n^2\pi^2} + \sqrt{\frac{b^2\beta^4}{4n^4\pi^4} + \frac{b\beta^2}{n^2\pi^2} - 1} \sin\left(n\pi\frac{\beta_0}{\beta}\right).\tag{53}$$

Now, let us investigate the solutions of (52) and (53) in detail. For simplicity we first discuss the motion near the extrema of the potential [cf. (37) and (38)]. For  $x = x^-$  the only

solution of the equation of motion is the constant solution  $x(\tau) = x^-$  with energy  $\epsilon = V^-$  for all temperatures. For  $x = x^+$  we see that for high temperatures there exists only one constant solution  $x(\tau) = x^+$  with  $\epsilon = V^+$  (see Fig.5a). When the temperature is lowered two new solutions appear at  $\tilde{\beta}_c < \beta_c$  describing oscillatory solutions to the left side of the well in the inverted potential with  $\dot{x}(0) < 0$ . Note that in the symmetric case  $\tilde{\beta}_c$  is always larger than  $\beta_c$ . The solution with amplitude  $x_m$  closer to  $x^+$  is unstable while the other solution is stable. For the stable path  $|x^+ - x_m|$  increases with decreasing temperature. When we arrive the temperature

$$\beta_{ab}(x^+) = \frac{4}{b} \sqrt{a + b \sinh(x^+)}, \quad (54)$$

where  $x_m$  reaches

$$x_{ab} = \operatorname{arsinh}(-a/b), \quad (55)$$

the energy  $\epsilon$  changes sign and the oscillatory solution changes into a segment of an unbounded trajectory. For  $\beta \rightarrow \infty$  the amplitude  $x_m$  tends to  $x^-$  (see Fig.5a). For the unstable solution the difference  $|x^+ - x_m|$  decreases with decreasing temperature until we arrive the critical temperature where  $\beta = \beta_c$ . There the unstable solution and the constant solution meet in a double bifurcation point. At  $\beta = \beta_c$  the constant solution becomes unstable and a new solution with growing amplitude appears. This stable path describes an oscillation to the right side in the well of the inverted potential. In an analogous way further bifurcations emerge with decreasing temperature.

Now, for  $x \neq x^+$  and  $x \neq x^-$  four cases must be distinguished. First, for  $x^- < x < x_{ab}$  the only paths connecting  $x$  and  $x'$  with  $x = x'$  are segments of unbounded trajectories with  $\epsilon < 0$ . These paths extend from high to low temperatures.

Second, in the case  $x > x^+$  we have at high temperatures only one solution with  $\dot{x}(0) > 0$  that extends continuously to low temperatures (see Fig.5a). As the temperature is decreased two new solutions with amplitudes  $x_m < x^+$  appear at a critical inverse temperature  $\tilde{\beta}_c$  describing oscillations to the left side of the well in the inverted potential (see Fig.5a). One

of these solutions is stable and the other one is again unstable. With increasing  $x$  the critical inverse temperature  $\tilde{\beta}_c$  also increases. At  $\beta = \beta_{ab}(x)$  (54) the stable oscillation changes to a segment of an unbounded trajectory with amplitude  $x_m$  that reaches  $x^-$  if  $\beta \rightarrow \infty$ . The amplitude  $x_m$  of the unstable path moves away from  $x^+$  with increasing  $\beta$  until we arrive the temperature where  $|x^+ - x_m| = x - x^+$ . At this point the path that is periodic in configuration space [ $x = x', \dot{x}(0) = -\dot{x}(\beta)$ ] becomes a path that is periodic in phase space [ $x = x', \dot{x}(0) = \dot{x}(\beta)$ ] (see Fig.5a). One can show that this new path and all further paths bifurcating with decreasing temperature are unstable.

Third, we consider the intermediate region  $x_{ab} < x < x^+$ . (52) defines a minimal inverse temperature  $\beta_c^+$  for which a bifurcation occurs. The corresponding boundary value  $\bar{x}$  is denoted by  $x_c^+$ . In the symmetric case ( $b = 0$ ) we find  $\beta_c^+ = \beta_c$  and  $x_c^+ = x^+ = 0$ , while in the asymmetric case the values  $\beta_c^+ < \beta_c$  and  $x_c^+ < x^+$  depend on the potential parameters  $a$  and  $b$  and have to be calculated numerically. Again two cases must be distinguished. If  $x_{ab} < x < x_c^+$  we have a bifurcation scenario similar to the former case  $x > x^+$ . On the other hand, in the case  $x_c^+ < x < x^+$ , the high temperature solution does not extend to low temperatures continuously. At an inverse temperature  $\beta_c^+ < \beta < \beta_c$  two new solutions with  $x_m < x^+$  emerge, a stable and an unstable path. When the inverse temperature is increased the unstable path and the high temperature solution meet at a bifurcation point and disappear while the new stable solution extends to low temperatures. Increasing the inverse temperature further another bifurcation of a stable and an unstable solution occurs, however, now with  $x_m > x^+$ .

Finally, for  $x < x^-$  again two cases have to be distinguished (see Fig.5b). For  $x$  near  $x^-$  the high temperature solutions continuously extend to low temperatures and no bifurcations occur. As  $x$  becomes smaller a bifurcation occurs for  $x = x_c^-$  at a critical inverse temperature  $\beta_c^- > \beta_c$  that may be determined from (52). This scenario remains true for all  $x < x_c^-$ . Then a stable and an unstable path bifurcate at a critical temperature. As the temperature is decreased further the unstable path meets the high temperature solution in a second bifurcation point while the stable path extends to the low temperature region (see Fig.5b)



In the general case  $x \neq x'$  the boundary conditions (47) may be evaluated in an analogous way and similar bifurcation sequences occur as the temperature is lowered.

### C. Classical Action and Fluctuation Determinant

Fortunately, not all extremal action paths have to be taken into account in the semiclassical approximation (42) for a given temperature since the corresponding classical actions are not always minima of  $S[x]$ . One gains from (40) and (46) for the action of the classical paths

$$S_{cl} = -\epsilon\beta + \frac{2}{\sqrt{2\epsilon}} \text{Re} \left[ \frac{f}{\sqrt{g^2 - h^2}} \left( \arctan \left\{ \frac{f \tan \left[ \sqrt{2\epsilon}(\beta + \beta_0)/2 \right] + h}{\sqrt{g^2 - h^2}} \right\} - \arctan \left\{ \frac{f \tan \left[ \sqrt{2\epsilon}\beta_0/2 \right] + h}{\sqrt{g^2 - h^2}} \right\} \right) \right] \quad (56)$$

where  $\text{Re}$  denotes the real part. In (56) we have introduced the complex coefficients

$$\begin{aligned} f &= \frac{1}{2}(b + ia) \\ g &= \frac{b}{4\epsilon} + i \\ h &= \sqrt{\frac{b^2}{16\epsilon^2} + \frac{a}{2\epsilon}} - 1, \end{aligned} \quad (57)$$

and the quantities  $\epsilon$  and  $\beta_0$  are determined by the boundary conditions (47). In the symmetric case ( $b = 0$ ) (56) reduces to

$$S_{cl} = -\epsilon\beta + \sqrt{a} \left( \arctan \left\{ \sqrt{\frac{a}{2\epsilon}} \tan \left[ \sqrt{2\epsilon}(\beta + \beta_0) \right] \right\} - \arctan \left\{ \sqrt{\frac{a}{2\epsilon}} \tan \left[ \sqrt{2\epsilon}\beta_0 \right] \right\} \right) \quad (58)$$

Considering first the case  $x = x' = x^+ = 0$  we have for  $\beta < \beta_c$  only the trivial solution  $\bar{x}(\sigma) = 0$  with the action

$$S_{cl}[0] = a\beta/2. \quad (59)$$

At  $\beta_c = \pi/\sqrt{a}$  two new branches emerge with the action

$$S_{cl}^{(1)} = \frac{\sqrt{a}}{2} \left( 2\pi - \frac{\pi^2}{\sqrt{a}\beta} \right) \quad (60)$$

which for  $\beta > \beta_c$  is smaller than  $S_{cl}[0]$ . Therefore, as mentioned above, we have a Hopf bifurcation at  $\beta = \beta_c$ . The other paths with  $x = x' = 0$  bifurcating at  $\beta = n\beta_c$  have the action

$$S_{cl}^{(n)}(\beta) = n S_{cl}^{(1)}\left(\frac{\beta}{n}\right). \quad (61)$$

Hence, the actions of the classical paths appearing at bifurcation points for temperatures  $\beta \geq 2\beta_c$  differ from  $S_{cl}^{(1)}$  by terms which are large compared to 1 in the semiclassical limit  $\hbar \rightarrow 0$ , which, more precisely, corresponds to the limit  $1/\sqrt{a} \rightarrow 0$  for the present case. As will be seen below, also in the asymmetric case at most two classical trajectories contribute to the semiclassical approximation of the equilibrium density matrix.

We now proceed to calculate the Gaussian fluctuations about the extremal action paths. After some algebra one obtains from (44) and (46) for the determinant  $J$

$$\begin{aligned} J = & \frac{2\pi}{\sqrt{2\epsilon}} \left( 1 + \left\{ \frac{b}{4\epsilon} + h \sin [\sqrt{2\epsilon}(\beta + \beta_0)] \right\}^2 \right)^{-1/2} \left( 1 + \left\{ \frac{b}{4\epsilon} + h \sin [\sqrt{2\epsilon}\beta_0] \right\}^2 \right)^{-1/2} \\ & \times \left[ \left( \frac{b^2}{8\epsilon^2} + \frac{a}{2\epsilon} \right) \sin [\sqrt{2\epsilon}\beta] + \frac{b}{2\epsilon} h \left\{ \cos [\sqrt{2\epsilon}\beta_0] - \cos [\sqrt{2\epsilon}(\beta + \beta_0)] \right\} \right. \\ & \left. - h^2 \sqrt{2\epsilon}\beta \cos [\sqrt{2\epsilon}\beta_0] \cos [\sqrt{2\epsilon}(\beta + \beta_0)] \right], \end{aligned} \quad (62)$$

with  $h$  from (57). Using (47) one can show that  $J$  is positive for the stable classical paths but negative for the unstable one. Of course, for unstable paths the fluctuation determinant is only defined as an analytical continuation, or formally by (42) and (43). Further, one sees that  $J$  vanishes at the inverse temperatures  $\beta = \tilde{\beta}_c$  where the new stable and unstable paths emerge. We note that (63) is also valid for  $\epsilon < 0$  by virtue of the relations  $\sin(ix) = i \sinh(x)$  and  $\cos(ix) = \cosh(x)$ . For instance, for  $x = x' = x^-$ , the only solution of (45) is given by  $\epsilon = V^-$  and the fluctuation determinant  $J$  reads

$$J[x^-] = \frac{2\pi}{\sqrt{2|V^-|}} \sinh \left( \sqrt{2|V^-|\beta} \right). \quad (63)$$

In particular, when we insert the trivial solution for  $x = x' = x^+$  into (47) one gets  $\epsilon = V^+$  and (62) reduces to

$$J[x^+] = \frac{2\pi}{\sqrt{2V^+}} \sin(\sqrt{2V^+}\beta) \quad (64)$$

which vanishes for  $\beta = \beta_c$  and is negative for  $\beta > \beta_c$ .

Let us now discuss the main features of the fluctuation determinant in the symmetric case ( $b = 0$ ). Qualitatively similar reasoning applies to the general case. For the stable branches with  $x = x^+ = 0$  bifurcating at  $\beta = \beta_c$  one finds for  $\beta > \beta_c$

$$J[x^+] = 2 \frac{2V^+\beta^3 - \pi^2\beta}{\pi} > 0. \quad (65)$$

This demonstrates the change of stability near  $\beta = \beta_c$  and shows that the simple semiclassical approximation becomes insufficient for temperatures close to  $\beta_c = \pi/\sqrt{2V^+}$ , i.e.  $T_c = \sqrt{2V^+\hbar^2}/\pi k_B m L_0^2$  in dimensional units.

At inverse temperature  $\beta = 2\beta_c$  and for boundary conditions  $x = x^+$  again two new classical paths bifurcate from the unstable trivial solution  $x(\sigma) = 0$ . However, using Eqs. (48) and (62), one sees that the corresponding determinant  $J$  is negative, while  $J[x^+]$  becomes positive for  $2\pi < \sqrt{2V^+}\beta < 3\pi$ . In function space this means that the paths newly emerging at  $\beta = 2\beta_c$  are unstable in one direction corresponding to one negative eigenvalue of the second order variational operator, see (43), while the trivial solution is unstable in two directions with two negative eigenvalues leading to a positive fluctuation determinant. More generally, one can show that all classical paths newly emerging for inverse temperatures  $\beta \geq 2\pi/\sqrt{2V^+}$  are unstable due to the fact that successively the eigenvalues  $\Lambda_n$  of the second order variational operator change from positive to negative values as the temperature is lowered. The only stable paths for inverse temperatures  $\beta > \beta_c$  are those bifurcating first near  $\beta = \beta_c = \pi/\sqrt{2V^+}$ . These paths are therefore the only ones contributing to the functional integral for lower temperatures in the semiclassical limit .

For temperatures close to  $T_c$  a change of stability occurs, as described above. The minimal action paths are then not well separated in function space and the semiclassical approximation according to (42) breaks down. This problem will be addressed in section 4.

### D. Semiclassical Density Matrix

Now, for high temperatures,  $\beta < \beta_c^+$  and given endpoints  $x, x'$  there is only one classical path with amplitude  $x_m$  which is obtained from (46) by choosing  $\epsilon$  and  $\beta_0$  according to (47). In practice,  $\epsilon$  and  $\beta_0$  have to be determined numerically. By virtue of Eqs. (56) and (62) the semiclassical density matrix for high temperatures,  $\beta < \beta_c^+$ , is then given by

$$\rho_\beta(x, x') = \frac{1}{Z} \frac{1}{\sqrt{J(x_m)}} e^{-S(x_m)}. \quad (66)$$

To illustrate this result we have depicted in Fig.6 the diagonal part of the density matrix  $P(x) = \rho_\beta(x, x)$  for the symmetric potential with  $b = 0$  in the semiclassical approximation (66) and the exact result (35) at inverse temperature  $\beta = \beta_c/2$  and for two values of  $a$ . Note that even for a small  $a = 4$ , the semiclassical approximation does rather well. The probability density  $P(x)$  is normalized by the condition  $\lim_{x \rightarrow \pm\infty} P(x) = 1$

For  $\beta \gtrsim \beta_c^+$  new classical paths may emerge, first for coordinates near the critical coordinate  $x_c^+$ . Then, one unstable path and two stable ones exist, determined by the solutions  $\epsilon$  and  $\beta_0$  of (47). Apart from a narrow region about the critical inverse temperature where the bifurcation occurs, these trajectories are well separated in function space and the sum in (42) contains the contribution of the two stable paths. The density matrix in the semiclassical approximation then reads

$$\rho_\beta(x, x') = \frac{1}{Z} \left[ \frac{1}{\sqrt{J(x_{m1})}} e^{-S(x_{m1})} + \frac{1}{\sqrt{J(x_{m2})}} e^{-S(x_{m2})} \right], \quad (67)$$

where we have denoted the amplitudes of the two stable paths with  $x_{m1}$  and  $x_{m2}$ . When  $S(x_{m1})$  exceeds  $S(x_{m2})$  by terms that are large compared to 1, it is inconsistent to take both contributions in (67) into account. In section 4 we will show that this is the case for all coordinates outside a narrow region around the barrier top and around the well region at  $x_c^-$ . Hence, mostly the functional integral is dominated by the contribution of one path and the semiclassical density matrix reduces to (66).

In Fig.7 the semiclassical approximation for  $P(x)$  calculated from (66) is depicted together with the exact result (35) at inverse temperature  $\beta = 2\beta_c$  for the potential (3) with

$a = b = 4$ . From (28) we see that there is only one bound state. Hence, in the semiclassical approximation deviations become apparent in the well region, while for the barrier region the semiclassical result gives an excellent approximation to the exact result. The semiclassical approximation in the well region becomes better if either  $a$  or  $b$  are increased corresponding to more bound states in the well. Only for coordinates in the vicinity of the barrier top the semiclassical approximation is given by the sum (67), which matches for larger  $x$  onto the simpler formula (66).

As we have seen above, the simple semiclassical approximation breaks down near those inverse temperatures  $\beta$  where bifurcations of the classical paths occur. As we will see in the next section this problem becomes relevant for coordinates in a narrow region around the barrier top, near the critical coordinate  $x_c^+$ , and in the well region, near the critical coordinate  $x_c^-$ . Only there, the simple semiclassical determination has to be improved due to the fact that the relevant classical paths are not well separated in function space. Furthermore, this analysis also gives the precise conditions for the validity of the formulae (66) and (67).

#### IV. SEMICLASSICAL DENSITY MATRIX NEAR CAUSTICS

The specific results presented in Figs. (6) and (7) are for temperatures well above or below the critical temperatures  $\beta_c^+$  and  $\beta_c^-$ , respectively, where the simple semiclassical results (66) and (67) are valid. A more refined treatment is required near the critical temperatures. In [6] we have shown how to determine the semiclassical density matrix in the critical region near the barrier top. Here, we shall apply these findings to the present problem.

Near the barrier top the potential (4) with  $a > 0$  may be expanded as

$$V(\xi) = V^+ \left[ 1 - \xi^2 + \frac{2}{3} a_3 \xi^3 + \frac{1}{2} a_4 \xi^4 + \mathcal{O}(\xi^5) \right], \quad (68)$$

where  $\xi = x - x^+$  and the potential parameters are given by

$$\begin{aligned} a_3 &= \frac{3}{2} \tanh(x^+) \\ a_4 &= \frac{4}{3} - \frac{5}{2} \tanh^2(x^+). \end{aligned} \quad (69)$$

Of course, for coordinates near the barrier top  $|\xi| \ll 1$ , and the anharmonic terms in Eq. (68) are much smaller than the parabolic one. However, for  $\beta \approx \beta_c^+$  they will be found to be crucial for the fluctuation integral even in the semiclassical limit.

To see this more clearly, we use the representation (43) of the determinant  $J$  as a product of eigenvalues of the second order variational operator. Representing the scaled quantum fluctuations in the form

$$y(\tau) = \frac{1}{\sqrt{2V^+}} \sum_{n=1}^{\infty} Y_n \sin\left(\frac{\pi n}{\beta} \tau\right), \quad (70)$$

we have shown in [6] that for high temperatures the second order variational operator is transformed to a diagonal matrix with eigenvalues

$$\lambda_n = \left(\frac{\pi n}{\sqrt{2V^+}\beta}\right)^2 - 1. \quad n = 1, 2, 3, \dots \quad (71)$$

Then, the path integral over the fluctuation modes reduces to a product of independent Gaussian integrals. By virtue of (43) and (71) one obtains our earlier result (64) for  $J$  by inserting the trivial solution.

Now, it is obvious that the Gaussian approximation becomes insufficient for inverse temperatures near  $\beta_c$  where the eigenvalue  $\lambda_1$  vanishes. As the temperature is lowered, the fluctuation mode amplitude  $Y_1$  increases with decreasing  $\lambda_1$ . As discussed in [6] the anharmonic terms lead to new stability and one gets for inverse temperatures near  $\beta_c$  for the action

$$S[x] - S[x_{\text{cl}}] = \frac{\beta}{4} \sum_{n=2}^{\infty} \lambda_n Y_n^2 + V(\xi_m, Y_1) \quad (72)$$

with the fluctuation potential

$$V(\xi_m, Y_1) = \frac{\beta}{4} \left\{ \left[ \lambda_1 - \lambda_c + \frac{9}{4} a_4 (\xi_m - \xi_{m,c})^2 \right] Y_1^2 + \frac{3a_4}{\sqrt{8V^+}} (\xi_m - \xi_{m,c}) Y_1^3 + \frac{3a_4}{16V^+} Y_1^4 \right\}. \quad (73)$$

Here, we have introduced the critical parameters

$$\xi_{m,c} = -\frac{32a_3}{27\pi a_4} \quad (74)$$

and

$$\lambda_c = \frac{9}{4}a_4\xi_{m,c}^2. \quad (75)$$

The coefficients  $a_3$  and  $a_4$  are given by (69). In (73)  $\xi_m$  is determined by the cubic equation

$$\frac{3}{4}a_4\xi_m^3 + \frac{8}{3\pi}a_3\xi_m^2 + \lambda_1\xi_m = \frac{2\pi}{\beta^2}(\xi + \xi'). \quad (76)$$

This equation has one or three real solutions corresponding to the one or three classical paths. In fact, for given endpoints near the barrier top the amplitudes  $x_m$  of the classical paths determined by (47) and  $V(x_m) = \epsilon$  are given by the roots of Eq. (76) according to  $x_m = \xi_m + x^+$ .

From Eq. (73) one sees that the coefficient

$$\Lambda_1(\xi_m) = \lambda_1 - \lambda_c + \frac{9}{4}a_4(\xi_m - \xi_{m,c})^2 \quad (77)$$

of the harmonic term may vanish, but the remaining terms of the fluctuation potential always constrain  $Y_1$  to fluctuation amplitudes at most of order  $(V^+)^{3/8}$ . Introducing the sum variable  $r = (\xi + \xi')/2$  we see from (76) that for given  $\beta$  the coefficient  $\Lambda_1(\xi_m)$  vanishes at values  $r = r_{\pm}$  (see Fig.8) where

$$r_{\pm}(\lambda_1) = r_c \left[ 3\frac{\lambda_1}{\lambda_c} - 2 \pm 2 \left( 1 - \frac{\lambda_1}{\lambda_c} \right)^{3/2} \right] \quad (78)$$

with

$$r_c = -\frac{3a_4V^+\beta^2}{8\pi}\xi_{m,c}^3. \quad (79)$$

Note, that  $r_c = x_c^+$  for  $\xi = \xi'$ . On the two curves  $r_{\pm}(\lambda_1)$  bifurcations of classical paths with endpoints near the barrier top occur according to the discussion in subsection 3.2.2. This analysis gives in detail the regions in the  $\lambda_1 - r$ -parameter space where one or three classical paths exist (see Fig.8).

For fixed  $\xi, \xi'$ , the potential  $V(\xi_m, Y_1)$  behaves as follows (see Fig.9). At high temperatures the fluctuation potential exhibits one minimum at  $Y_1 = 0$  according to one real

solution of (76). When the temperature is lowered to the value where  $r_{\pm}(\lambda_1) = r$  two new extrema arise at  $Y_1 \neq 0$ . Then, the fluctuation potential shows two minima and one local maximum. In the region in coordinate–temperature space around  $(r_c, \lambda_c)$  where  $|\Lambda_1(\xi_m)|$  is smaller than order  $(V^+)^{-1/4}$  both minima differ by terms which are smaller than order 1 and are not separated by a local maximum exceeding the minima by terms which are larger than order 1.

In this region the functional integral over the fluctuation modes now takes the form [6]

$$\int \mathcal{D}[y] e^{(S-S_c)[y]} = \sqrt{\frac{\lambda_1 \sqrt{2V^+}}{2\pi \sin(\sqrt{2V^+}\beta)}} K(\xi_m) \quad (80)$$

with the fluctuation integral

$$K(\xi_m) = \sqrt{\frac{\beta}{4\pi}} \int_{-\infty}^{\infty} dY_1 e^{-V(\xi_m, Y_1)} \quad (81)$$

describing the contribution of the marginal mode  $Y_1$ . The fluctuation integral is finite for positive and negative values of  $\lambda_1 - \lambda_c$ .

By virtue of (56) and (80) the dimensionless density matrix near the top of the barrier potential (4) and in the vicinity of  $\lambda_1 = \lambda_c$  takes the form

$$\rho_{\beta}(x, x') = \frac{1}{Z} \sqrt{\frac{\lambda_1 \sqrt{2V^+}}{2\pi \sin(\sqrt{2V^+}\beta)}} K(\xi_m) e^{-S(x_m)}. \quad (82)$$

Usually, explicit results for the distribution can be calculated only numerically. After solving (76) for given  $\lambda_1$  and  $\xi, \xi'$  one has to insert  $\xi_m$  into the fluctuation potential (73) and determine the fluctuation integral (81). All steps involve only rather simple numerics. Outside the critical region where  $|\lambda_1 - \lambda_c| \lesssim (V^+)^{-1/4}$  and  $|\xi|, |\xi'| \lesssim \max(a_3(V^+)^{-1/4}, (V^+)^{-3/8})$  the result (82) smoothly matches onto the various semiclassical approximations specified above in (66) and (67). In particular, one can show [6] that for coordinates outside the critical region, the minimum of the fluctuation potential  $V(\xi_m, Y_1)$  corresponding to the globally stable path differs from the other minimum by terms which are large compared to 1. Therefore, for coordinates outside the critical region the density matrix is given by (66).



For coordinates near the barrier top, (66) must be used for  $\lambda_1 - \lambda_c > (V^+)^{-1/4}$ , (67) for  $\lambda_1 - \lambda_c < (V^+)^{-1/4}$ , and (82) in between.

In principle, the procedure to determine the fluctuation integral (80) for critical coordinates in the well region near  $x_c^-$  is similar to the case studied above. As we have seen in section 3, a stable and an unstable path newly emerge at the caustic (see Fig. 5b). These paths with endpoints near  $x_c^-$  have amplitudes  $x_m$  with large  $|x_m - x_c^-|$ . Hence, the trajectories explore the nonlinear range of the well region and the eigenfunctions of the second order variational operator cannot be calculated analytically. However, the features of the fluctuation potential are the same as discussed above for the caustic near  $x_c^+$ . Thus the fluctuation integral can also be determined in the following way. First, since there is one unstable path, the determinant  $J$  in (62) contains only one vanishing eigenvalue at the caustic. Second, well beyond the caustic one has one or two stable classical paths which are well separated in function space so that the density matrix is given by (66) and (67). Finally, the equation for the boundary values (47) expanded around the critical coordinate  $x_c^-$  and the critical temperature  $\beta_c^-$  yields in leading order a cubic equation similar to (81) for  $\xi_m = x_m - x_{m,c}$  where  $x_{m,c}$  is the corresponding amplitude at the critical point. The critical values  $x_c^-$  and  $\beta_c^-$  are determined by (47) and derivatives thereof. Hence, similar to (78), the fluctuation potential near the critical point may be written in the form

$$V(x_m, Y) = \frac{1}{2}J(x_m)Y^2 + \frac{1}{3}J_3Y^3 + \frac{1}{4}J_4Y^4 . \quad (83)$$

Here,  $J(x_m)$  denotes the determinant of the second order variational operator of a stable classical path with amplitude  $x_m$  and  $Y$  is proportional to the amplitude of the marginal fluctuation mode. The coefficients  $J_3$  and  $J_4$  are determined by the corresponding cubic equation. Then, the density matrix near the caustic is given by

$$\rho_\beta(x, x') = \exp[-S(x_m)] \int_{-\infty}^{\infty} \frac{dY}{\sqrt{2\pi}} \exp[-V(x_m, Y)], \quad (84)$$

where  $S(x_m)$  is the action (56). The regions in temperature–coordinate–space where the various semiclassical formulas have to be used may be determined in a way analogous to the analysis near the barrier top.

Fig. 10 shows the divergent simple semiclassical result (66), the improved formula (82), and the exact result (35) for the position distribution  $P(x)$  at temperature  $\beta = \beta_c^+$ . The exact result and the improved formula differ by terms which are at most of order  $1/\sqrt{2V^+}$ .

The formulas (82) and (84) for the improved semiclassical approximation combines with the formulas (66) and (67) for the usual semiclassical approximation to yield the semiclassical equilibrium density matrix for all temperatures. In particular, the position distribution for very low temperatures will be discussed in the next section.

## V. SEMICLASSICAL BOUND STATES AND RESONANCES

From (34) one sees that for low temperatures the density matrix is dominated by the contributions of bound states while the contribution of the extended states is exponentially suppressed. For large  $\beta$  we expect large deviation between the semiclassical approximation (67) and the exact result (35) due to the fact that differences between the exact and semiclassical energy eigenvalues of the bound states are exponentially amplified in the corresponding Boltzmann factors for  $\beta \rightarrow \infty$ . However, we will show in the following that the semiclassical position distribution can nevertheless be used to determine the absolute square of the wave functions  $|\Psi_n(x)|^2$ ,  $n = 0, 1..n_{max}$  of the bound states with energies  $E_n$ ,  $n = 0, 1..n_{max}$  reasonably well.

For very low temperatures the position distribution function is, apart from exponentially small corrections, dominated by the ground state. Thus, the low temperature limit enables us to extract the absolute square of the ground state wave function from the shape of  $P_\beta(x)$ . Additionally, from the low temperature behavior of the maximum of  $P_\beta(x)$  in the well region we can extract the semiclassical energy eigenvalue of the ground state  $E_0$  by use of the formula

$$E_0 = \frac{1}{\Delta\beta} \lim_{\beta \rightarrow \infty} \ln \left[ \frac{P_\beta(x_{max})}{P_{\beta+\Delta\beta}(x_{max})} \right], \quad (85)$$

where  $x_{max}$  denotes the coordinate where  $P_\beta(x)$  has its maximum. The wave function  $|\Psi_0(x)|^2$  is then given by  $\exp(\beta_0 E_0) P_{\beta_0}(x)$  where  $\beta_0$  has to be chosen sufficiently large so

that this product becomes independent of temperature [14]. This procedure can be extended also to the next excited state in the following way. We subtract the contribution of the ground state from the probability distribution at a higher temperature  $\beta_1$  where  $\beta_1$  has to be chosen large enough so that the reduced position distribution

$$P_{1,\beta}(x) = P_\beta(x) - |\Psi_0(x)|^2 \exp(-\beta E_0) \quad (86)$$

is dominated by the first excited state. From the reduced probability distribution we extract the first excited state  $|\Psi_1(x)|^2$  and its energy  $E_1$ . Accordingly, we get a sequence of temperatures  $\beta_0 > \beta_1 > \beta_2 > \dots$  and reduced probabilities  $P_{n,\beta}(x)$  from which we can find the semiclassical approximation for the wave functions  $|\Psi_n(x)|^2$  and the energies  $E_n$ . To illustrate this, we depict in Fig. 11a the exact (27) and semiclassical ground state wave function  $|\Psi_0(x)|^2$  for an antisymmetric potential with potential parameters  $a = 0$  and  $b = 4$ . For these parameters there is only one bound state (cf. (26)) with the semiclassical energy  $E_0 = -0.326\dots$ , while the exact energy eigenvalue from (29) is  $\epsilon = -0.459\dots$ . The temperature chosen to define the ground state is  $\beta_0 = 12$ . Note that the wave function is very well reproduced, while the Boltzmann factors differ largely:  $\exp(\beta_0(E_0 - \epsilon_0)) \simeq 5$ .

The semiclassical density matrix can also be used to study scattering states, in particular resonances. As we have seen in the previous sections the semiclassical approximation of the equilibrium density matrix does rather well even for systems that have only a few bound states except for very low temperatures where the amplification of errors in the energy eigenvalues has to be taken into account. From the exact solution of the equilibrium density matrix we know that the contribution of the scattering states exhibits several peaks. These resonances correspond to energy "eigenstates" with complex eigenvalues. In Fig. 11b we depict the exact and semiclassical position distribution (upper curves) as well as the reduced position distribution  $P_{1,\beta}(x)$  (86)(lower curves) for the same set of parameters as in Fig. 11a at temperature  $\beta = 0.5$ . Since for these parameters there is only one bound state,  $P_{1,\beta}(x)$  represents the contribution of the scattering states to the position distribution. According to the single bound state in the potential, the distribution  $P_{1,\beta}(x)$  shows one resonance

peak which is a typical quantum mechanical effect of interference of scattering states. The semiclassical approximation, based on purely imaginary time mechanics, reproduces the resonance very well.

#### **ACKNOWLEDGMENTS**

The authors would like to thank E. Pollak for enspiring discussions. This work was supported in part by the Deutsche Forschungsgemeinschaft through SFB 276.

## REFERENCES

- [1] M. V. Berry, and K. E. Mount, *Rep. Prog. Phys.* **35**, 315 (1972); M. C. Gutzwiller, *Chaos in Classical and Quantum Mechanics*, (Springer-Verlag, New York, 1990).
- [2] H. Grabert, P. Olschowski, and U. Weiss, *Phys. Rev. B* **36**, 1931 (1987); P. Hänggi, P. Talkner, and M. Borkovec, *Rev. Mod. Phys.* **62** (1990) 251; J. Ankerhold, H. Grabert, and G. L. Ingold, *Phys. Rev. E* **51**, 4267 (1995); J. Ankerhold, and H. Grabert, *Phys. Rev. E* **52**, 4704 (1995).
- [3] R.P. Feynman and A.P. Hibbs, *Quantum Mechanics and Path Integrals* (McGraw-Hill, New York, 1965). R. P. Feynman, *Statistical Mechanics* (Benjamin, New York, 1972); L.S. Schulman, *Techniques and Applications of Path Integrals* (Wiley, New York, 1981); H. Kleinert, *Path Integrals in Quantum Mechanics, Statistics, and Polymer Physics* (World Scientific, Singapore, 1990).
- [4] W. H. Miller, *J. Chem. Phys.* **55**, 3146 (1971); *ibid.*, **58**, 1664 (1973); R. M. Stratt, and W. H. Miller, *J. Chem. Phys.* **67**, 5894 (1977).
- [5] M. J. Gillian, *J. Phys. C* **20**, 3621 (1987); G. Voth, D. Chandler, and W. H. Miller, *J. Chem. Phys.* **91**, 7749 (1989); J. Cao, and G. A. Voth, *J. Chem. Phys.* **100**, 5093 (1994); *ibid.*, **100**, 5106 (1994); *ibid.*, **101**, 6157 (1994); *ibid.*, **101**, 6168 (1994);
- [6] J. Ankerhold, and H. Grabert, *Physica A* **188**, 568 (1992); F. J. Weiper, J. Ankerhold, and H. Grabert, *Physica A* **223**, 193 (1996).
- [7] C. Eckart, *Phys. Rev.* **35**, 1303 (1930).
- [8] L. D. Landau and E. M. Lifschitz, *Quantum Mechanics* (Pergamon, Oxford, 1977).
- [9] P. M. Morse, *Phys. Rev.* **34**, 57 (1929); N. Rosen, and P. M. Morse, *Phys. Rev.* **42**, 210 (1932).
- [10] Formally, the dimensionless units introduced are obtained by putting  $m = \hbar = L_0 = 1$ .

- [11] Note that this transformation differs from the customary ansatz  $y = \tanh(x)$  for the Eckart and Rosen–Morse potentials. The latter transformation is not useful for potential (3) if  $b \neq 0$ .
- [12] M. Abramowitz, and I. A. Stegun, *Handbook of Mathematical Functions* (U. S. GPO, Washington, D. C.,1964).
- [13] J. Ankerhold, F.-J. Weiper, and H. Grabert in: H. Grabert et al. (eds.), *Path Integrals from meV to MeV* (World Scientific, Singapore 1993).
- [14] Note that we have to normalize  $P_\beta(x)$  with  $Z=1$  for this procedure, i.e.  $\lim_{x \rightarrow \pm\infty} P_\beta(x) = (2\pi\beta)^{-1/2}$ .

## FIGURES

FIG. 1. The potential (3) for various potential parameters  $a$  and  $b$ .

FIG. 2. The transmission probability (6) as a function of  $b$  for fixed potential parameter  $a = 1$  and various energies  $\epsilon$ .

FIG. 3. The transmission probability (6) as a function of  $a$  at fixed energy  $\epsilon = 0.015$  for various potential parameters  $b$ .

FIG. 4. Bifurcation diagram for the amplitude  $x_m$  of the classical path  $x(\tau)$  versus the dimensionless inverse temperature  $\beta$  for potential parameters  $a = 1, b = 0$ . The solid lines are the stable and the dashed lines are the unstable branches for a pure ( $x = x' = 0$ , thick lines) and a perturbed ( $x = x' > 0$ , thin lines) bifurcation.

FIG. 5. The asymmetric bifurcation scenario for various boundary conditions and potential parameters  $a = 1, b = 5$ . a) The thick lines represents the amplitude  $x_m$  for  $x = x^\pm$ , the thin lines represent the amplitude  $x_m$  for  $x > x^+$ . The solid (dashed) lines represent the stable (unstable) paths. b) The amplitude  $x_m$  for the boundary values (from above)  $x^- > x > x_c^-$ ,  $x = x_c^-$  and  $x < x_c^-$

FIG. 6. Position distribution  $P(x)$  for a symmetric barrier potential ( $b = 0$ ) at inverse temperature with  $\beta = \beta_c/2$  for (a)  $a = 4$  and (b)  $a = 25$ . The solid lines represent the exact result (35) and the dotted lines the semiclassical formula (66).

FIG. 7. Position distribution  $P(x)$  at inverse temperature  $\beta = 2\beta_c$ . The potential parameters are  $a = b = 4$ . The solid line represents the exact result (35), the dashed lines the semiclassical formula (66).

FIG. 8. The  $\lambda_1$ - $r$ -plane is divided by the two curves  $r_\pm(\lambda_1)$  (solid lines) into two regions in which the cubic equation (76) has one or three (shaded region) solutions. Along the line  $r_e(\lambda_1)$  one has  $\xi_m = \xi_{m,c}$ .

FIG. 9. The fluctuation potential (73) for  $\xi_m = \xi_{m,c}$  and inverse temperatures near  $\beta_c$ .

FIG. 10. Position distribution  $P(x)$  for a symmetric barrier potential with  $a = 25$  and  $b = 0$  at the critical inverse temperature  $\beta_c^+ = \pi/5$ . The solid line represents the exact result (35), the dashed line the divergent semiclassical formula (66), and the dotted line the improved semiclassical result (90).

FIG. 11. a) The absolute square of the ground state wave function for an antisymmetric barrier potential with  $a = 0$  and  $b = 4$ . b) The position distribution  $P(x)$  (upper curves) and the resonance (lower curves) for the same set of potential parameters at inverse temperature  $\beta = 0.5$ . The solid lines represents the exact results, the dashed lines the semiclassical ones.



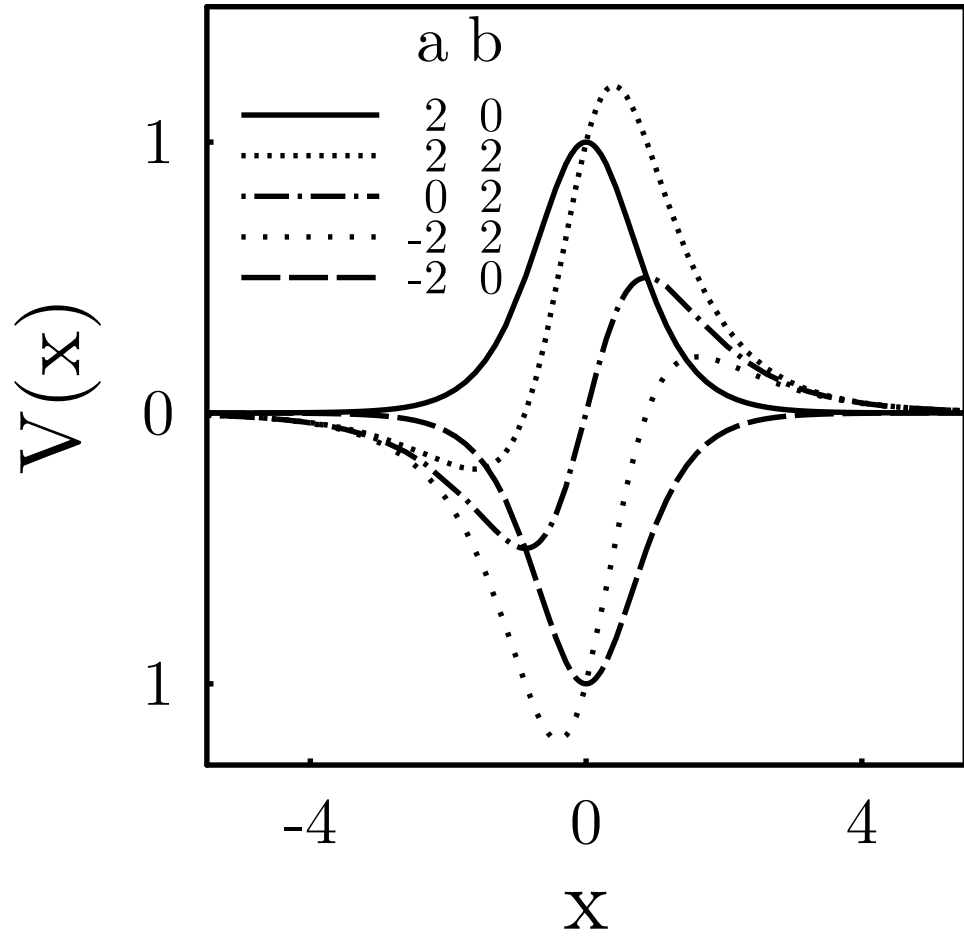


Figure 1, F. J. Weiper et al.

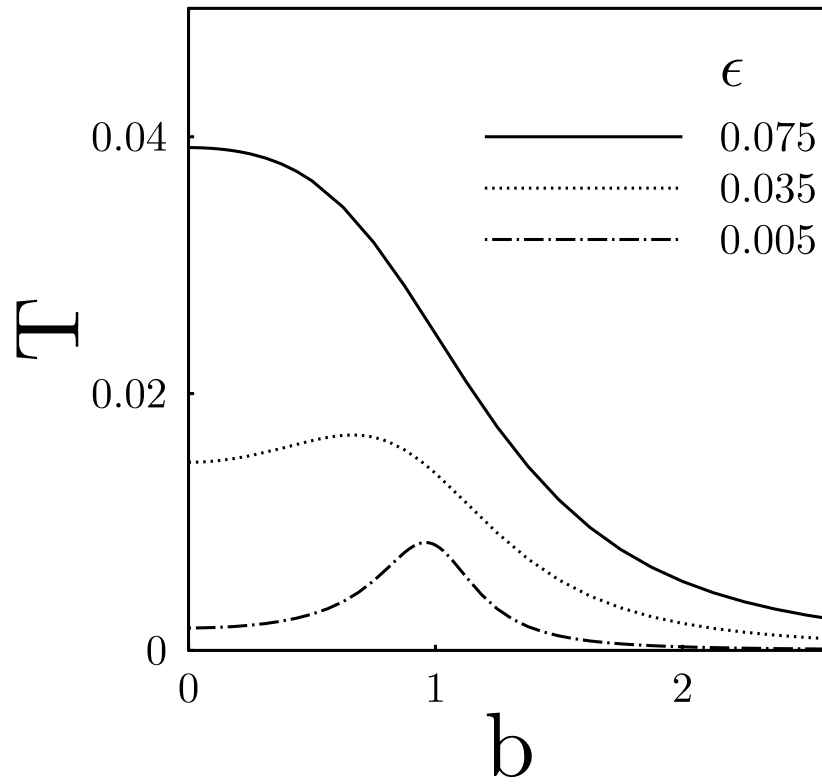


Figure 2, F. J. Weiper et al.

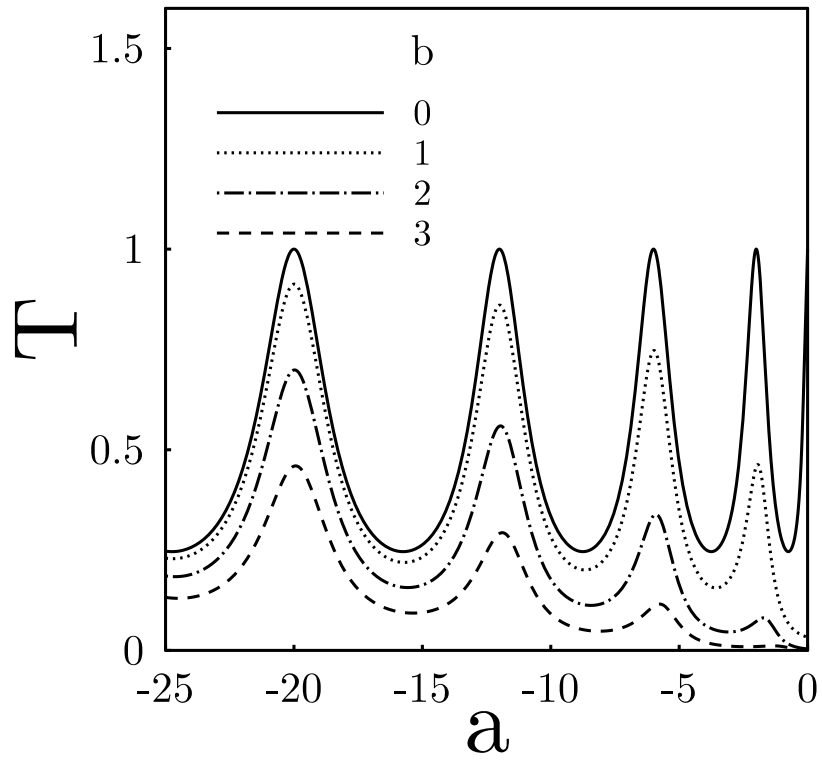


Figure 3, F. J. Weiper et al.

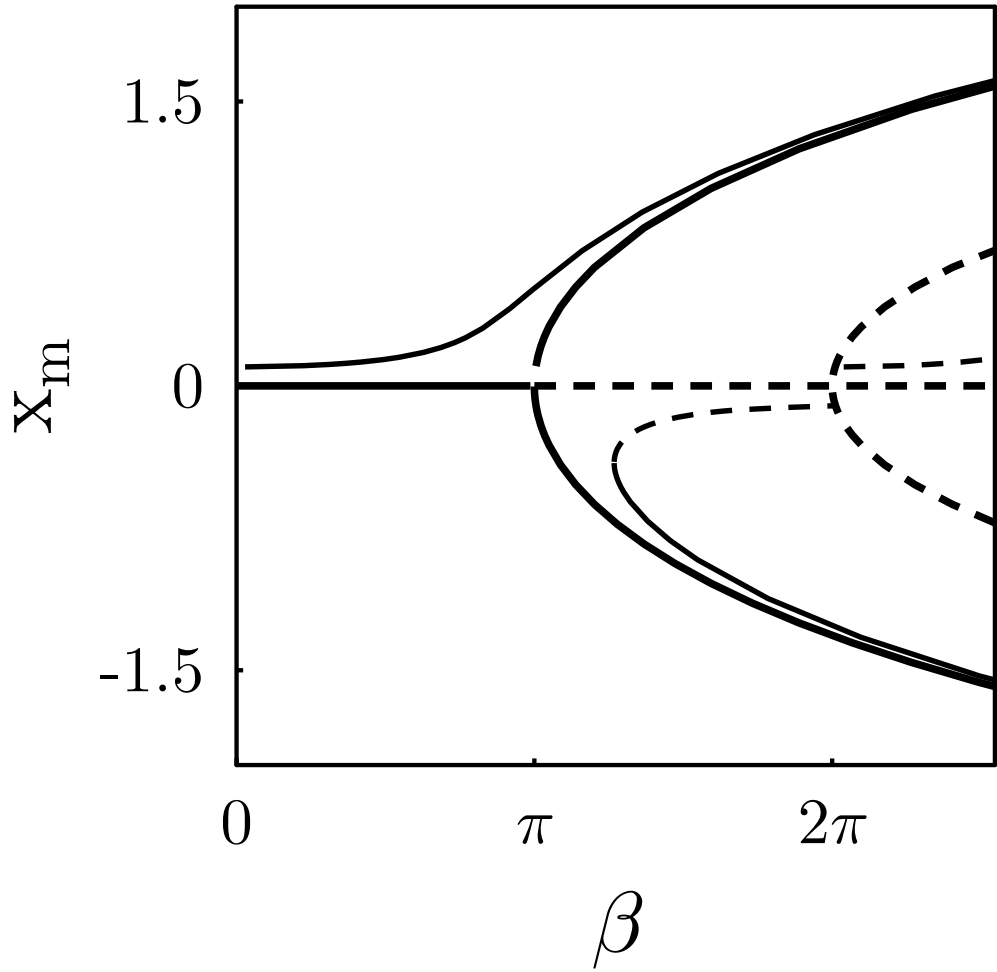


Figure 4, F. J. Weiper et al.

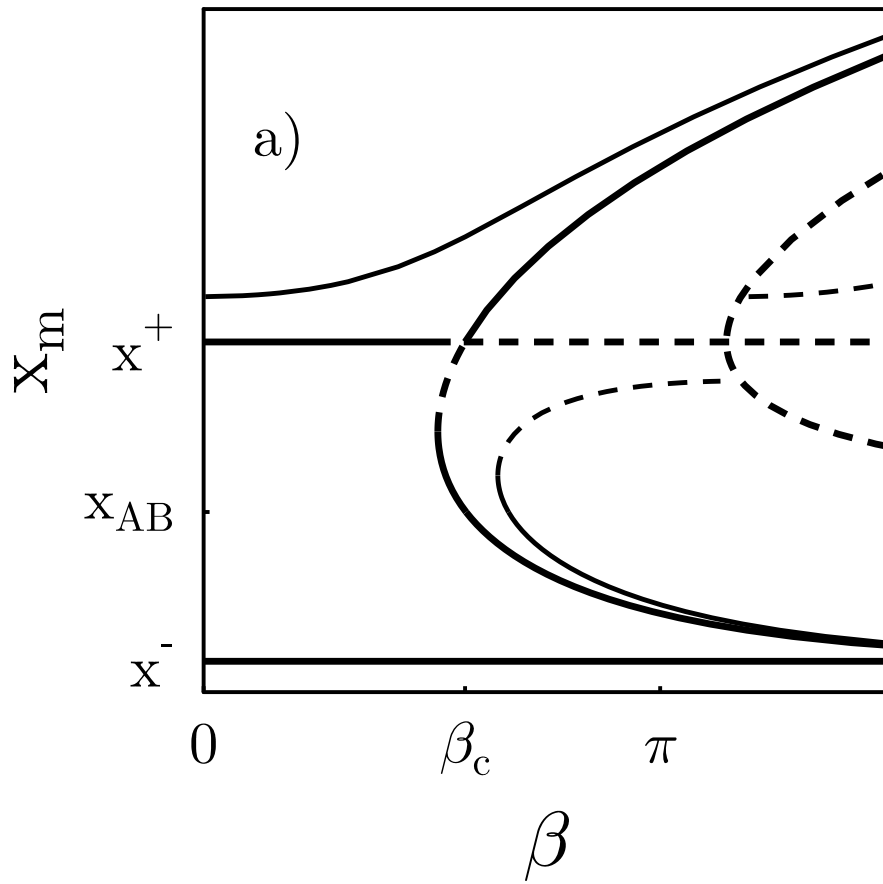


Figure 5a, F. J. Weiper et al.

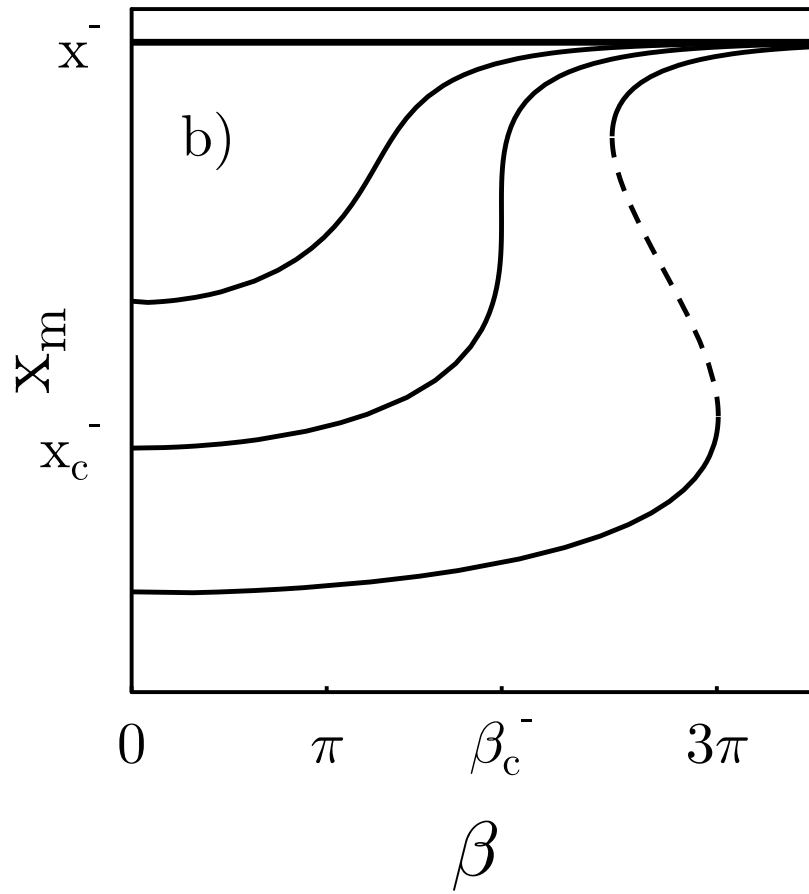


Figure 5b, F. J. Weiper et al.

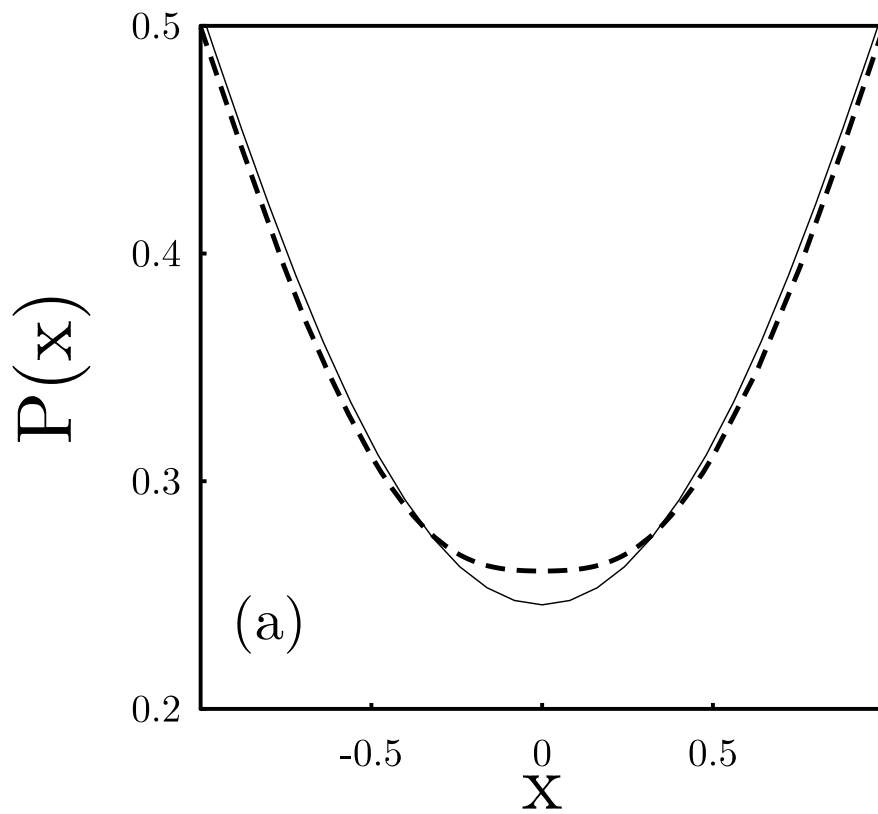


Figure 6a, F. J. Weiper et al.

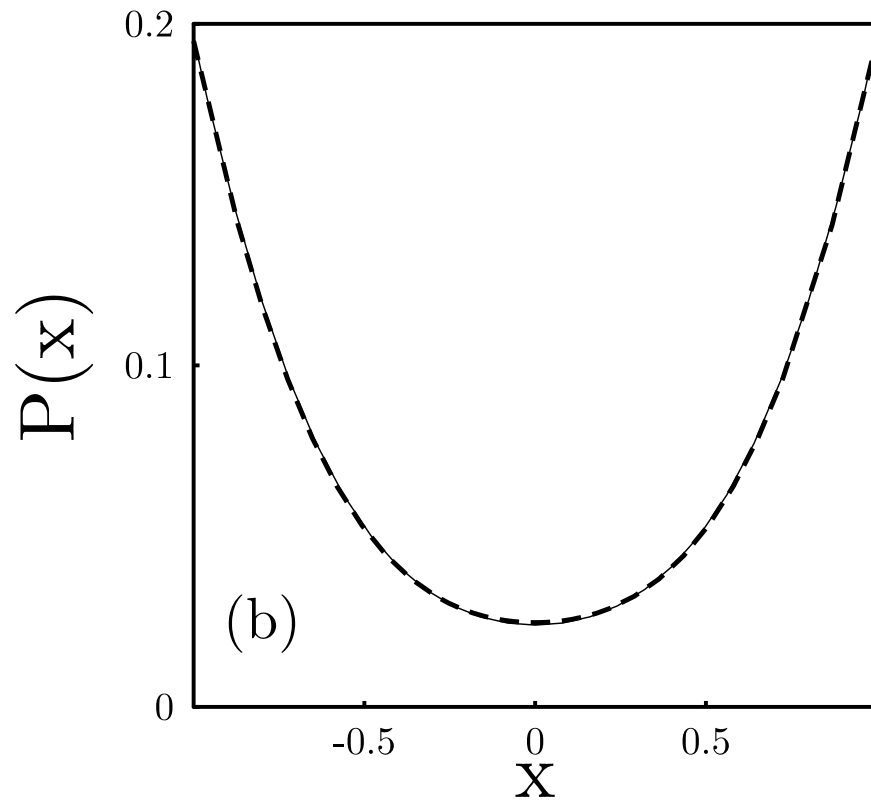


Figure 6b, F. J. Weiper et al.



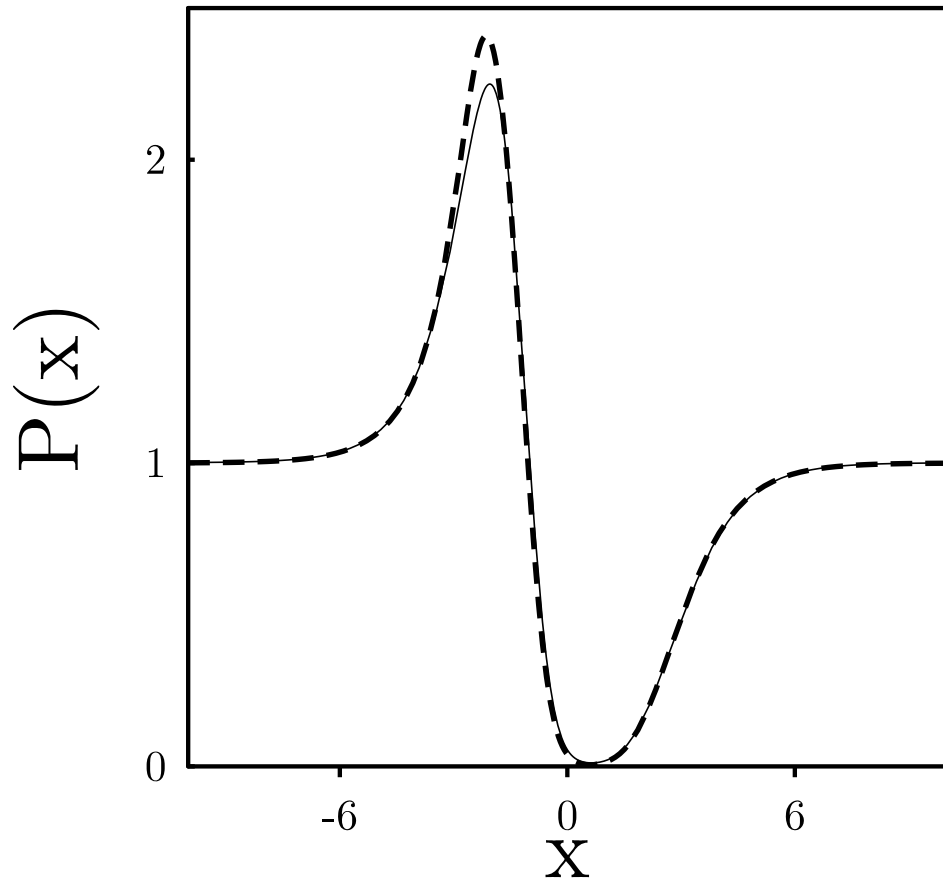


Figure 7, F. J. Weiper et al.

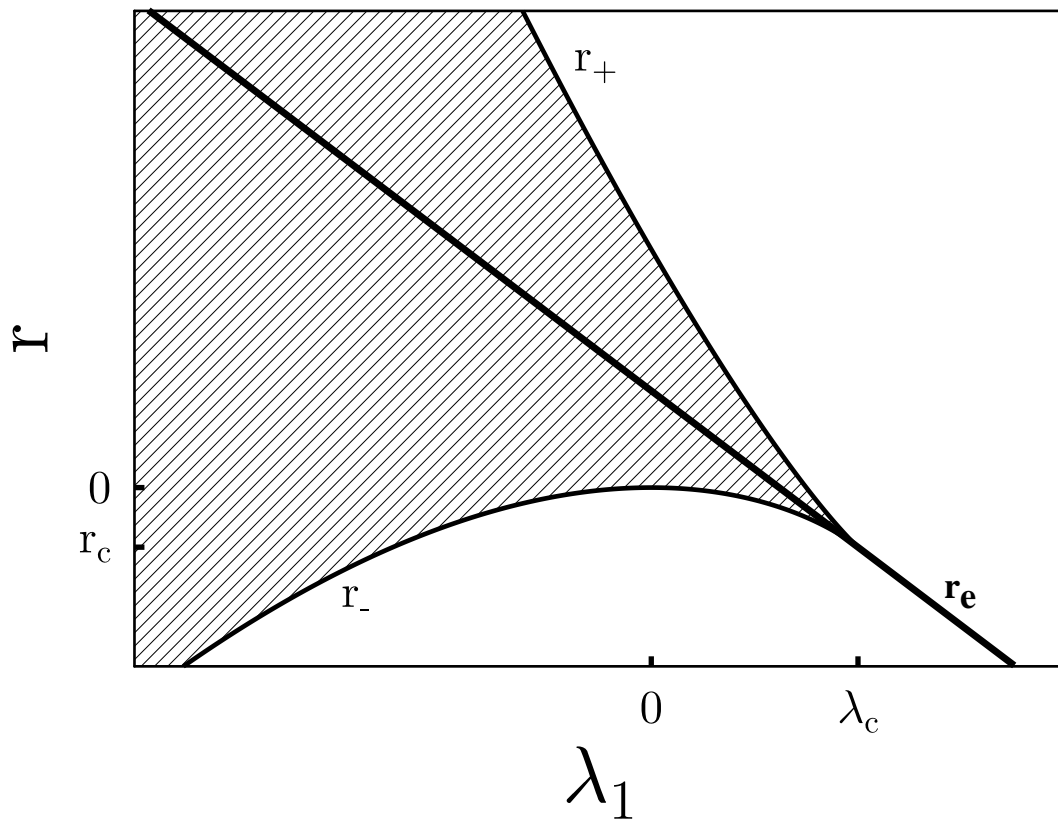


Figure 8, F. J. Weiper et al.

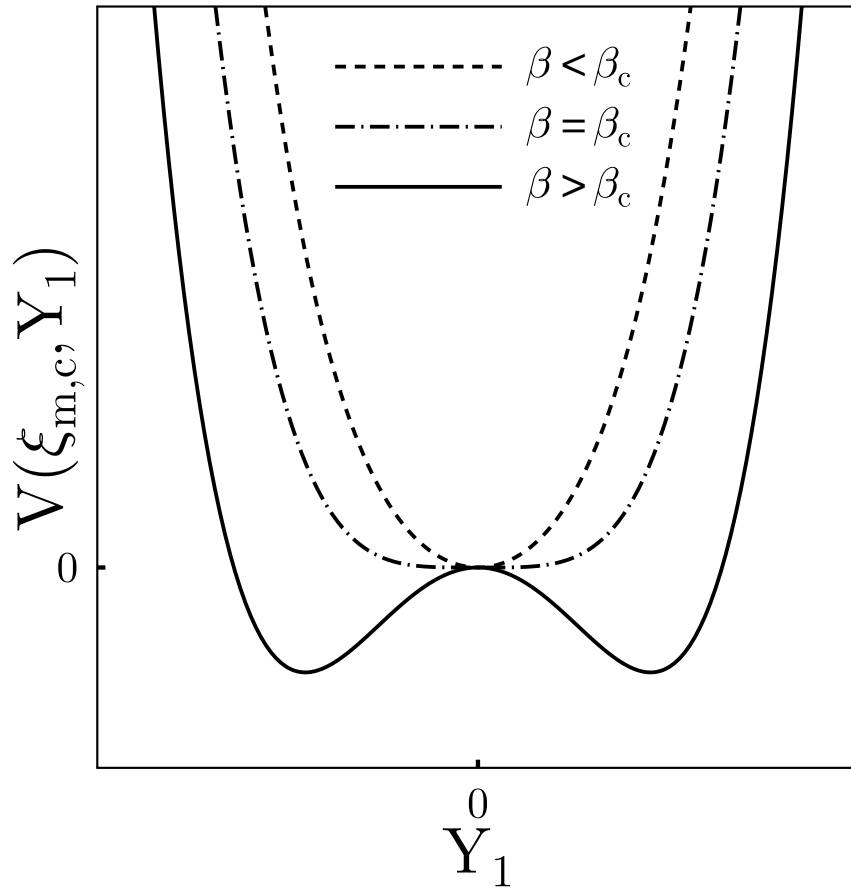


Figure 9, F. J. Weiper et al.

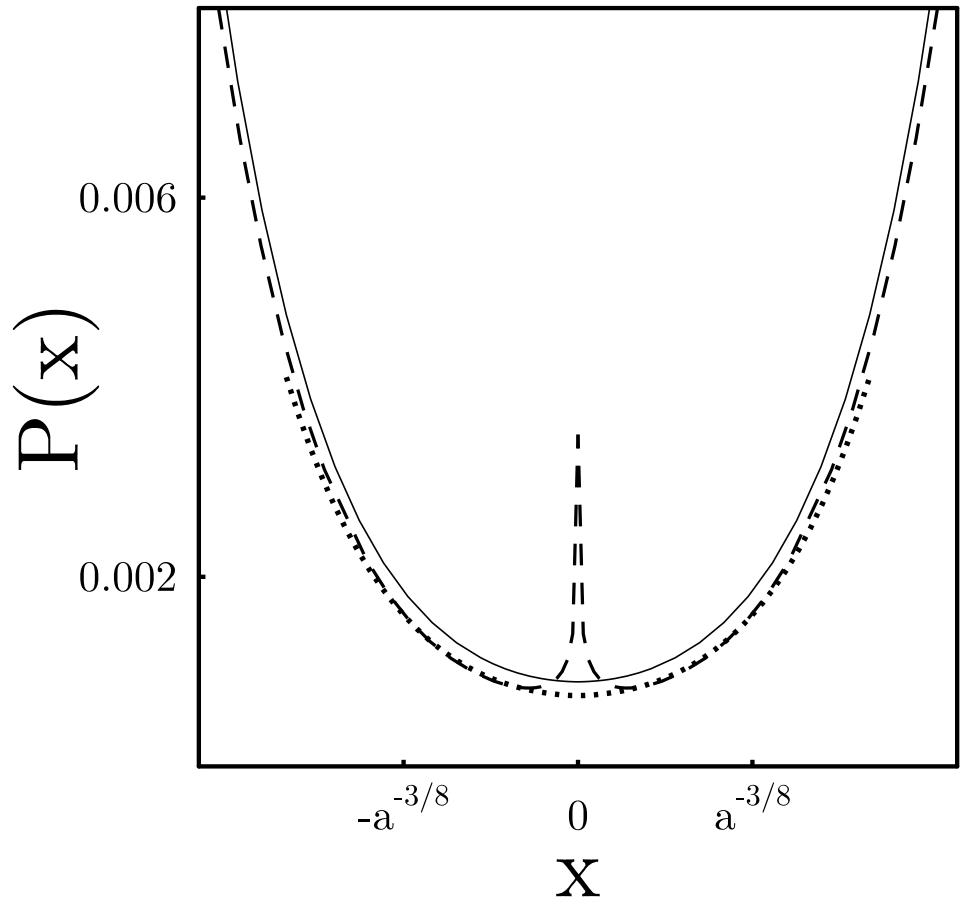


Figure 10, F. J. Weiper et al.

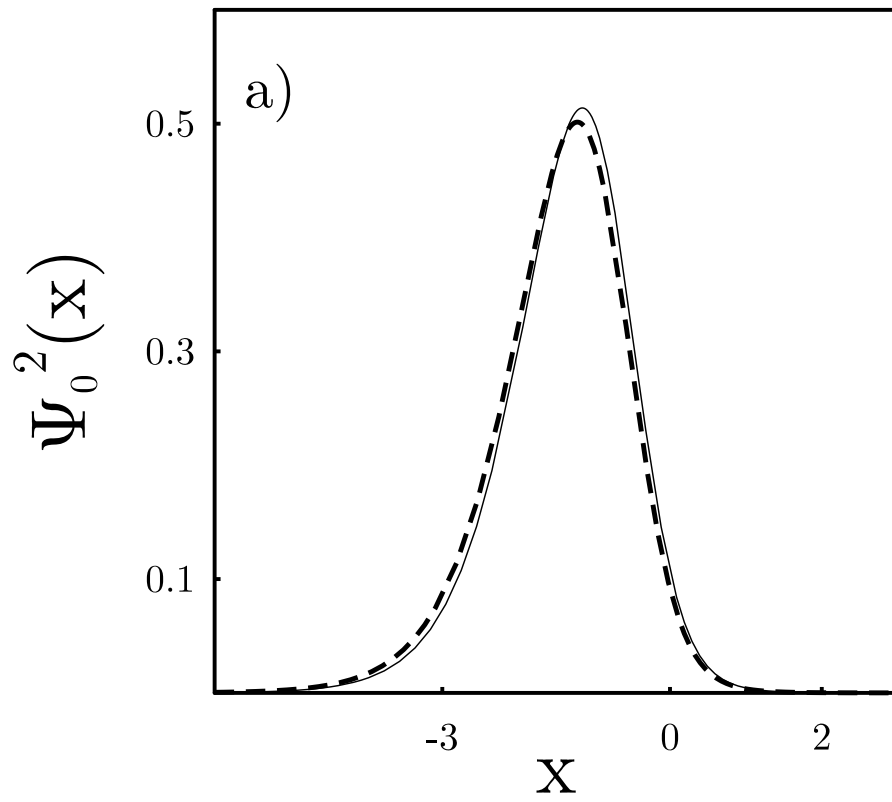


Figure 11a, F. J. Weiper et al.

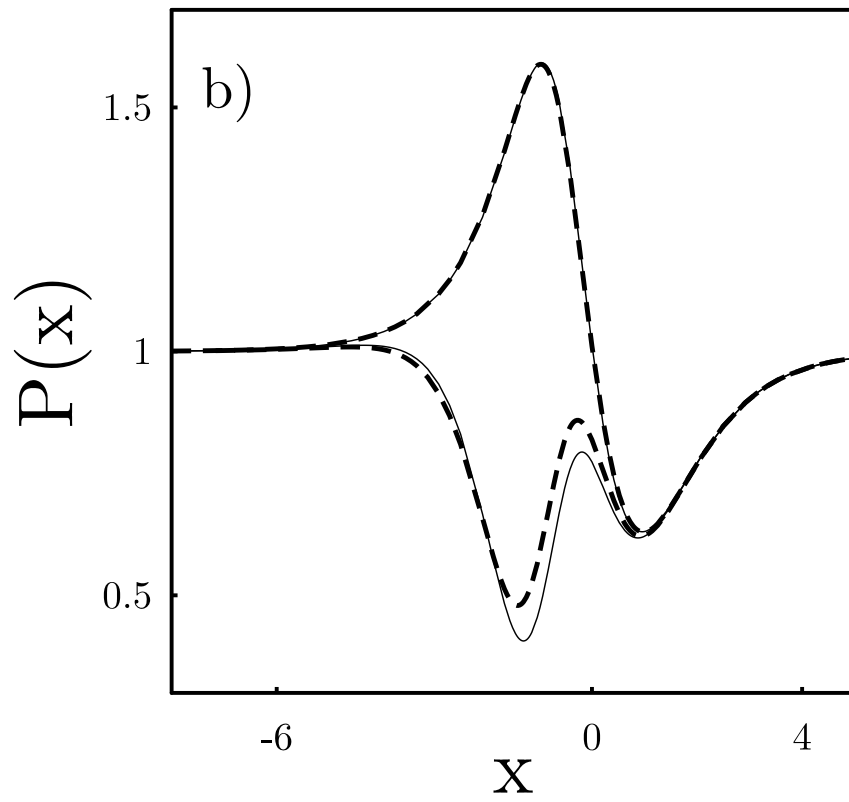


Figure 11b, F. J. Weiper et al.